

A bootstrap method for gain calibration and resolution determination of a lead-glass calorimeter

R.T. Jones^{a,1}, M. Kornicer^a, A.R. Dzierba^b, J.L. Gunter^{b,2}, R. Lindenbusch^b, E. Scott^b,
P. Smith^b, C. Steffen^{b,3}, S. Teige^{b,*}, P. Rubin^{c,4}, E.S. Smith^d

^aDepartment of Physics, University of Connecticut, Storrs, CT 06268, USA

^bDepartment of Physics, Indiana University, Bloomington, IN 47405, USA

^cDepartment of Physics, University of Richmond, Richmond, VA 23173, USA

^dThomas Jefferson National Accelerator Facility, Newport News, VA 23606, USA

Received 5 May 2006; received in revised form 29 July 2006; accepted 29 July 2006

Available online 23 August 2006

Abstract

We describe a method for calibration of a lead-glass calorimeter that does not require a beam of known energy. The technique was used to calibrate the RADPHI lead-glass calorimeter at Jefferson Lab. The technique described can be applied to any segmented electromagnetic calorimeter capable of detecting all-photon decays of mesons, for example, $\pi^0 \rightarrow 2\gamma$, $\eta \rightarrow 2\gamma$ or $\omega \rightarrow \pi^0\gamma$. We also demonstrate how the measured 2γ mass width of the π^0 and η mesons can be unfolded to extract the single-shower energy and position resolution functions of the calorimeter.

© 2006 Elsevier B.V. All rights reserved.

PACS: 25.20.Lj; 14.40.Cs

Keywords: Meson; Photoproduction; Radiative; Decay; Phi; Radphi; Calorimeter; Calibration

1. Introduction

The photon detector built for the RADPHI experiment [1] at the U.S. Department of Energy's Thomas Jefferson National Accelerator Facility (Jefferson Lab) was designed to detect and measure all-photon decays of ϕ mesons photoproduced in a 50 MHz tagged bremsstrahlung photon beam. The primary component of this detector was a 620-element lead-glass electromagnetic calorimeter. This paper describes methods to determine the calibration

and resolution characteristics of the detector without the use of a beam of known energy.

The lead-glass detector (LGD) is shown in Fig. 1. It consisted of $4\text{ cm} \times 4\text{ cm} \times 45\text{ cm}$ blocks arranged in a 28×28 cell array with an approximately circular shape. The long axes of the blocks were oriented parallel to the beam. The four central blocks were removed to permit the unscattered photon beam to pass to the photon beam dump. The array was instrumented with type FEU-84-3 phototubes. A one-piece support structure held the phototubes in place relative to the lead-glass array, one tube per block, with each phototube viewing its corresponding lead-glass block across a small air gap.

The front face of the LGD was positioned 103 cm downstream from the target and subtended an angle of approximately 27° from the beam line. The target was a Beryllium cylinder of length 2.53 cm, and diameter 2.87 cm. The compact target allowed the interaction vertex to be approximated as the target center. The interactions of interest produced photons with energies up to 5 GeV,

*Corresponding author. Tel.: +1 812 855 4623.

E-mail address: steige@indiana.edu (S. Teige).

¹RADPHI Spokesman, 2001-present.

²Present address: Departments of Diagnostic Radiology and MR Research Laboratory, Mayo Clinic, Rochester, MN 55905, USA.

³Present address: National Center for Supercomputing Applications, Champaign, IL 61820, USA.

⁴Present address: Department of Physics and Astronomy, George Mason University, Fairfax, VA 22030, USA.

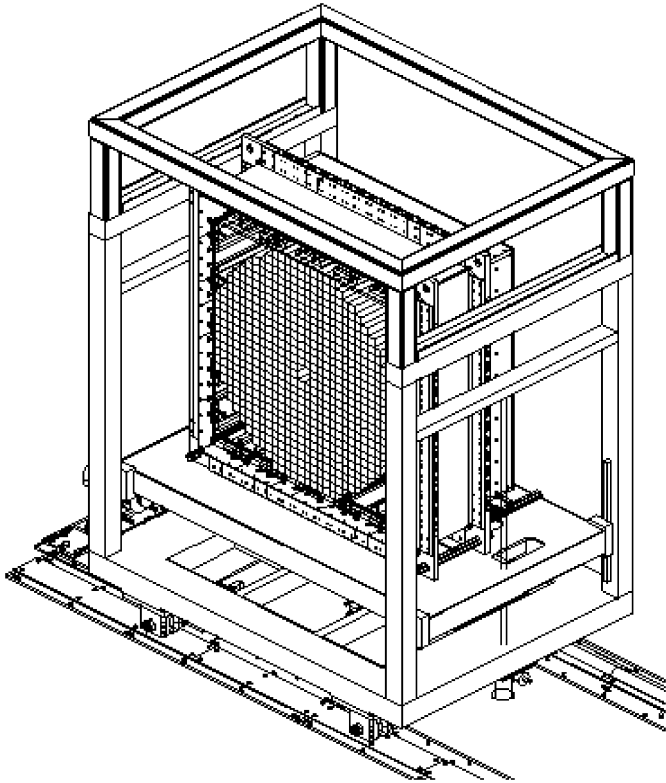


Fig. 1. The LGD mounted on its transporter; the glass stack is shown with the uninstrumented corner blocks removed for clarity.

generating electromagnetic showers that occupied several calorimeter cells. Photons with energies as low as 100 MeV could be reconstructed.

2. Shower reconstruction

2.1. Cluster finding

The photons to be reconstructed in the calorimeter are the decay products of mesons produced by interactions of the photon beam in the small cylindrical Beryllium target. Approximating the initial point of all produced photons as the center of the target, the direction of a photon is determined by the position of any space point along the axis of the shower generated by the photon in the calorimeter. The determination of the four-vector is completed by measuring the energy of the photon.

A photon incident on the calorimeter deposits energy in several neighboring LGD blocks. The first step in reconstructing the photon four-vector is to identify the blocks which shared the energy deposited by the electromagnetic shower.

The algorithm to associate groups of blocks into “clusters” has three steps.

In the first step, the algorithm searched the list of LGD block pulse heights for the block with the largest energy deposition, called the “seed” block. Neighboring blocks containing deposited energy are associated with the seed

block to form a cluster. This procedure is then repeated to form clusters from the remaining blocks in the list. In each step, one considers only “active” blocks, i.e. those which are not already associated with clusters. Initially all blocks with ADC values over pedestal are active. Once one cluster is completed, the blocks in the cluster are removed from the list of active blocks and the process is repeated until the highest-energy block remaining is below some minimum seed energy, chosen to correspond to 150 MeV. At this stage the found clusters are no larger than 3×3 blocks and not all blocks in the active list are used, i.e. associated with a cluster.

In the second step, the clusters are expanded by incorporating unused blocks contiguous with clusters into the original groups. If a block is near two step-1 clusters, the block is associated with both clusters, its energy shared in proportion to the energy contained in the central portion of the clusters.

The third step repeats the first step but allows a seed block to have a lower minimum energy, chosen to correspond to 50 MeV. Once all possible seed blocks are exhausted, the cluster-finding procedure is finished.

2.2. Shower position and energy corrections

To a first approximation, the total energy of a reconstructed shower is equal to the sum of the observed energy in each of the blocks that belong to a cluster. For showers near normal incidence, improved resolution can be obtained by introducing a small nonlinear correction that takes into account a few-percent increase in the response of lead glass to showers above 1 GeV because of attenuation and light-collection efficiency effects in the blocks [2]. For showers at incidence angles above about 15° , however, the shower energy and centroid positions are coupled, requiring a more sophisticated approach.

To find the direction of the photon, a vector is constructed beginning at the center of the target and ending at the point (X_c, Y_c, Z_m) where X_c and Y_c are the measured coordinates (discussed below) of the shower centroid in the transverse plane of the LGD and Z_m is the estimated longitudinal coordinate of the maximum of the shower profile inside the LGD. The direction and energy of the photon that created the shower are written in spherical coordinates as (E, θ, ϕ) where θ is the polar angle with respect to the beam direction and ϕ is the azimuthal angle in the transverse plane. At incidence angles of order 10° the reconstructed direction depends mainly on (X_c, Y_c) and is insensitive to Z_m , while the dependence of reconstructed E on Z_m can be absorbed into the nonlinear correction described above. At incidence angles above 15° , however, the dependence of the reconstructed photon momentum on Z_m must be taken into account explicitly. The acceptance of RADPHI depends upon reconstructing showers as far as 25° from the normal. Furthermore, at angles beyond 20° there are increasing effects from shower leakage out of the sides of the array, which introduces a bias in both the

photon direction and the energy, if this effect is not properly taken into account.

The analysis presented below relies on a detailed Monte Carlo shower simulation to map in three dimensions from unknowns (θ, ϕ, E) , to measured values (X_c, Y_c, S) where E is the true energy of the photon and S is the observed energy summed over the cluster. Incident photons are generated in the target covering a fine grid in both direction and energy. These photons are simulated in a GEANT-based Monte Carlo simulation with full shower generation. The resulting events are then analyzed using the standard cluster algorithm described above to find the average centroid and observed energy for each grid point. This map is parameterized using an expansion in a suitable set of basis functions to obtain algebraic forms for $X_c(\theta, \phi, E)$, $Y_c(\theta, \phi, E)$, and $S(\theta, \phi, E)$. This system of equations can be inverted using an iterative method to provide corrected estimates for (θ, ϕ, E) for each reconstructed shower. This solution has a limited radius of convergence in polar angle θ . For angles greater than 22° , increasing the value of E beyond a certain limit actually corresponds to a decreased S (see Fig. 2) because of increased shower leakage for higher-energy showers. This leads to an effective upper bound on the energies of large-angle showers that can be reconstructed in such a calorimeter. For RADPHI this limit was 1 GeV at 24° , decreasing to 100 MeV at 26° . Fortunately for the RADPHI experiment, the energy spectrum of photons at these angles from all-neutral decays of vector mesons has very little yield above 500 MeV, so below 25° this cutoff did not appreciably affect the acceptance of the experiment.

A slice through the function $S(\theta, \phi, E)$ at $\phi = 0$ and a range of values for E is shown in Fig. 2. The data points in the figure represent the average reconstructed shower energy for the given generated sample. The error bars show the r.m.s. spread in the reconstructed values that come from photoelectron statistics and shower fluctuations. The curve is the algebraic parameterization that emerged from a fit to a generic form for $S(\theta, \phi, E)$.

The Monte Carlo shower simulation relies on the standard GEANT3 [3]. Inside the LGD blocks the response of the lead glass is simulated in detail by explicit creation and following of individual Cherenkov photons as they are produced in the development of the shower. The Cherenkov spectrum in the simulation is bounded at long wavelength by the response of the photocathode (cuts off above 700 nm) and at short wavelength by the attenuation curve of lead glass (cuts off below 400 nm). Between these two bounds, the photocathode efficiency, the attenuation of lead glass and the refractive index are all included with their known wavelength dependence. Cherenkov light is polarized and the reflection and transmission of the polarized light is treated exactly in the simulation. The typical Cherenkov photon undergoes a number of reflections before reaching the photocathode or being absorbed. Wrapping the blocks with a thin layer of air between the glass surface and the surrounding aluminized mylar layer

was an important factor in the simulation, as was the presence of an air gap at the interface between the block and the phototube. One consequence of the latter is that light emitted at the critical Cherenkov angle of 52° by a particle moving parallel to the block axis has zero probability of being detected at the phototube; these photons are entirely contained inside the block by total internal reflection.

Two important consequences follow from this observation. The first is that the overall shower response goes through a local minimum at normal incidence, where a large fraction of the shower particles are in the “blind spot” with radiating shower particles nearly parallel to the block axis. The simulation showed that at 20° the light output from a 1 GeV shower was about 20% greater than at normal incidence. The second consequence is that the observed lateral size of a shower must be larger than the size expected based upon the shower energy deposition profile. This follows from the fact that the most energetic particles in a shower are found near the center of the shower profile and these are the particles whose directions are most likely parallel to the block axis. The observed light yield coming from the core of the shower distribution is thus suppressed relative to light coming from the shower periphery where particle energies are lower and directions are more random. In fact, there was a discrepancy of nearly 50% between observed shower size in RADPHI data and Monte Carlo before this angle-dependent collection efficiency was understood. After the effect was included in the simulation, the shapes of real and simulated showers were compared in terms of spatial moments up to the fourth moment and they were found to be in agreement within measurement errors.

The reduced photoelectron yield observed at small angles in Fig. 2 is associated with photons entering the beam hole of the LGD. These photons encounter only a portion of the lead-glass block and hence generate a reduced number of photoelectrons.

3. Calibration

The operating voltage, and hence the gain, of the phototubes was initially selected by illuminating the detector with a pulsed laser. This procedure equalized the gains to within a factor of two. These cell to cell variations were eliminated by an offline calibration described below.

The LGD calibration procedure makes use of prominent peaks in the multi-photon effective mass spectra corresponding to known mesons decaying into multi-photon final states, e.g. π^0 , η and ω . These peaks are already identifiable in the reconstructed mass spectra before the gain calibration has been carried out, even when individual tubes vary in gain by as much as a factor of 2. The gains were set during the experimental run by adjusting the high voltage on individual tubes until their responses to an injected light pulse from the calibration laser were approximately equalized. The pulser equalization proce-

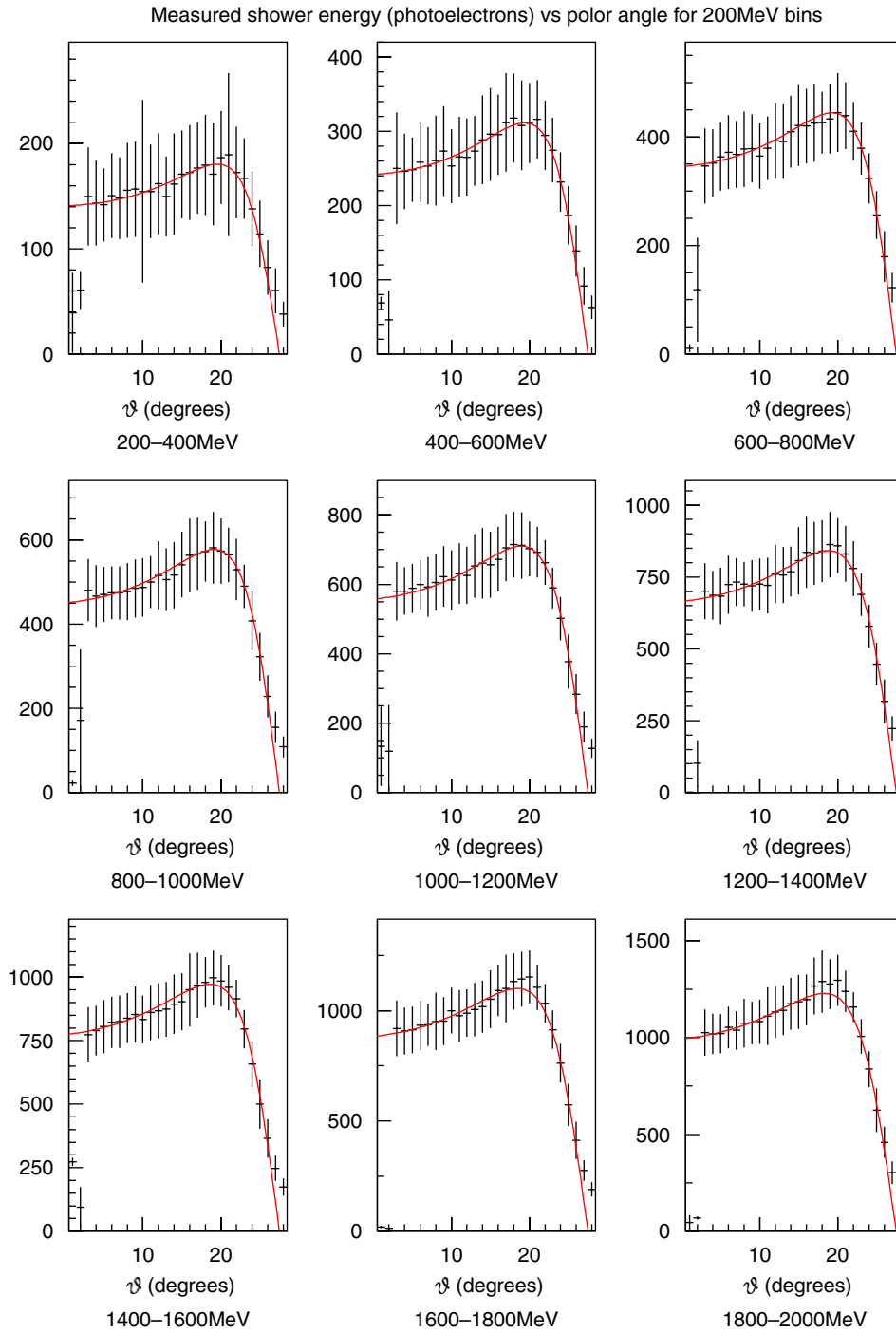


Fig. 2. Simulated photoelectron yield in the RADPHI LGD as a function of polar angle θ for photons generated in the target at $\phi = 0$. The generated shower energies are distributed uniformly within the respective energy intervals. The data points are the average and r.m.s. yields for a sample of several hundred simulated showers. The curve is a fit to the data.

ture was repeated periodically throughout the run to take into account changes in the response of individual blocks arising from radiation damage and other sources of long-term drift during the experiment. Inhomogeneities in the calibration laser distribution system led to physical gains on particular channels that differed in some cases by more than a factor of two from the mean, with a 30% r.m.s.

deviation. The goal of the off-line calibration is to measure these gain factors with a precision significantly better than 5% using experimental data, so that they can be used to correct the ADC data prior to photon reconstruction.

Quantitatively, this is accomplished by adjusting individual gain factors of each LGD block to find the extremum

of a single global function of the data,

$$F = \sum_{i=1}^N (m_i^2 - m_0^2)^2 + 2\lambda \sum_{i=1}^N (m_i^2 - m_0^2) \quad (1)$$

where N is the number of events in the calibration data sample and i denotes a single event in that sample. The masses m_0 and m_i are the physical mass of the meson being used for the calibration and the reconstructed mass in the LGD for event i , respectively. The first term in F measures the width of the reconstructed mass peak, while the second term is introduced with the Lagrange multiplier λ to embody the constraint $\langle m_i^2 \rangle = m_0^2$.

The most convenient meson for calibration is the π^0 which appears as the dominant structure in the 2γ invariant mass plot for 2-cluster events. All events that were reconstructed with exactly two clusters and whose invariant mass lay within $\pm 30\%$ of the center of the observed π^0 peak were included in the calibration sample. The 2γ invariant mass-squared is given by

$$m_i^2 = 2p_{1i}p_{2i}(1 - \cos \gamma_i) \quad (2)$$

where $p_{1i,2i}$ are the reconstructed energies of the two showers, γ_i is the angle between the directions of the two showers as viewed from the target. The reconstructed energy p_{ji} is given by the observed energy s_{ji} in shower j , but contains additional nonlinear corrections.

The effects of the angle-dependent shower response correction can be expressed in terms of a factor g ,

$$p_{ji} = (1 + g) \sum_k E_{ji}^{(k)} = (1 + g)s_{ji} \quad (3)$$

where k labels an individual block contributing deposited energy $E_{ji}^{(k)}$ to shower j and the sum is over blocks contained in the cluster associated with the photon under consideration. The correction factor g is weakly dependent on the observed shower energy s_{ji} but does not depend on the block energies $E_{ji}^{(k)}$ individually. The calibration proceeds in an iterative manner, where one step consists of introducing a small channel-dependent gain correction factor ε_k such that $E_{ji}^{(k)} \rightarrow E_{ji}^{\prime(k)} = (1 + \varepsilon_k)E_{ji}^{(k)}$.

Minimizing F in Eq. (1) directly with respect to the variables ε_k is made difficult by the nonlinear dependence of m_i^2 on the block energies that appears in the factor g in Eq. (3) and also in the angle γ_i between the photons. Small shifts in the gain of a single channel, however will have a negligible effect on the correction g or the shower directions, but will rescale the p_{ji} of its shower. Hence the primary effect of the gain adjustment factor ε_k on the reconstructed photon momentum is to simply modulate its magnitude. It follows from this approximation that

$$\frac{\partial p_{ji}'}{\partial \varepsilon_k} \simeq p_{ji} \frac{E_{ji}^{(k)}}{s_j}, \quad (4)$$

$$\frac{\partial m_i^2}{\partial \varepsilon_k} \simeq m_i^2 \frac{E_{ji}^{(k)}}{s_j}. \quad (5)$$

These approximations lead to a linear equation which is satisfied at the extremum of the function F .

$$\begin{aligned} \frac{\partial F'}{\partial \varepsilon_k} &= 2 \sum_{i=1}^N (m_i^2 - m_0^2) \frac{\partial m_i^2}{\partial \varepsilon_k} + 2\lambda \sum_{i=1}^N \frac{\partial m_i^2}{\partial \varepsilon_k} \\ &= 2 \sum_{i=1}^N \left(m_i^2 - m_0^2 + \lambda + \sum_{k'} \varepsilon_{k'} \frac{\partial m_i^2}{\partial \varepsilon_{k'}} \right) \frac{\partial m_i^2}{\partial \varepsilon_k} \\ &= 0. \end{aligned} \quad (6)$$

The solution is given by

$$\varepsilon_k = [C^{-1}]_{kk'} (D - \lambda L)_{k'} \quad (7)$$

where

$$C_{kk'} = \sum_{i=1}^N \left(\frac{\partial m_i^2}{\partial \varepsilon_k} \frac{\partial m_i^2}{\partial \varepsilon_{k'}} \right),$$

$$D_k = - \sum_{i=1}^N \left((m_i^2 - m_0^2) \frac{\partial m_i^2}{\partial \varepsilon_k} \right),$$

$$L_k = \sum_{i=1}^N \frac{\partial m_i^2}{\partial \varepsilon_k}$$

and the value of λ is fixed by the condition that the centroid of the reconstructed mass peak must lie at the physical mass:

$$\lambda = \frac{B + L^T C^{-1} D}{L^T C^{-1} L} \quad (8)$$

where B is the mass bias $\sum_{i=1}^N (m_i^2 - m_0^2)$. Starting off with a uniform nominal gain factor for all channels, individual channel gain corrections are calculated using Eq. (7) and applied iteratively until the procedure converges to $\varepsilon_k \rightarrow 0$ for all k .

In practice, it was found that special care must be taken in the way that the matrix C is inverted. C is a square symmetric matrix of dimension the number of blocks in the calorimeter (620 in the case of RADPHI) whose elements are determined statistically by sampling a finite sample of N calibration events. Even for very large samples there are instabilities that appear when taking the inverse C^{-1} which demand careful treatment. The nature of these instabilities can be best understood by expressing C^{-1} in terms of its spectral decomposition,

$$[C^{-1}]_{kk'} = \sum_{\alpha} \frac{1}{c(\alpha)} e_k(\alpha) e_{k'}(\alpha) \quad (9)$$

where $c(\alpha)$ are the eigenvalues and $e(\alpha)$ the corresponding orthonormalized eigenvectors of C . Of the complete set of eigenvalues of C , there are generally a few whose values are very small and statistically consistent with zero. These terms tend to dominate the behavior of C^{-1} if it is calculated using exact methods. A better approach instead is to truncate Eq. (9) and include only eigenvectors in the sum whose eigenvalues are statistically well determined by the data. This truncation implicitly recognizes that there

are some linear combinations of the gains which cannot be determined from the given data sample, and simply leaves them unchanged from the initial conditions. Good convergence is generally obtained for samples of size 10^5 events or more after 8–10 iterations.

4. Resolution

The observed width of narrow mesons such as the π^0 and η that undergo 2γ decay is determined by the single-shower energy and position resolutions of the calorimeter. The relative contributions of the energy and position resolutions of the calorimeter to its mass resolution for electromagnetic decays depend upon the part of $n\gamma$ phase space where the decay takes place. Because shower centroid resolution is more or less independent of the separation between the two showers, the fractional error on the two photon opening angle γ will generally be larger when the two showers are close together in space than when they are far apart. It follows from Eq. (2) that position resolution effects on the mass resolution of the calorimeter are most important for events where the relevant showers are close to each other on the face of the calorimeter, and less important for events with well separated showers. By analyzing events of these two types separately and comparing results, it is possible to separate the two effects and extract the single-shower energy and position resolutions of the calorimeter based only on $n\gamma$ invariant mass spectra.

This idea was applied to the RADPHI data sample in the following way. First it was determined using Monte Carlo simulations that, under the conditions of the RADPHI experiment, the mass resolution of the η in its 2γ decay mode is dominated by the energy resolution of the calorimeter, and is insensitive to the shower position resolutions. By contrast, the π^0 mass resolution receives approximately equal contributions from the single-shower position and energy resolutions. To begin the resolution determination, we started with a sample of exclusive $\gamma p \rightarrow 2\gamma p$ events and selected pairs with one of the two showers in a narrow energy window and examined the energy spectrum of the other as a function of cluster-separation angle. After a sufficiently narrow cut on separation angle, this energy spectrum shows peaks that correspond to the masses of the π^0 and η whose line-shapes are convolutions of the energy response functions for the two showers plus the contribution from uncertainties on the shower centroid positions. The contribution from spatial resolution to the width of the peaks was minimized by focusing first on the η , which is associated with pairs of showers that are well separated on the face of the calorimeter. By analyzing the dependence of the peak width on the energies of the individual showers, the convolution was inverted to obtain the r.m.s. resolution for single showers as a function of shower energy without assuming any model for the energy dependence. Once the energy resolution had been determined in this way, the spatial resolution was then examined by looking at the

excess width of the π^0 peak over what was expected based upon energy resolution alone. In the end, a unified analysis including both energy and spatial resolution effects was able to reproduce both the π^0 and η profiles.

Proceeding as outlined above, the analysis begins by selecting a 2γ sample where the energy of one shower (label it shower 1) is required to be 2.00 ± 0.05 GeV. A second cut is made in the opening angle between the two showers of $\gamma = (16 \pm 0.5)^\circ$, and the energy spectrum of shower 2 is plotted. This spectrum contains one monochromatic peak of energy 1.93 GeV, assuming that there is a significant flux of ≈ 4 GeV η 's in the 2γ sample. The width of the monochromatic peak corresponds to the quadratic sum of the r.m.s. energy resolutions of the two showers, which in this case is $\sqrt{2}$ times the single-shower resolution of the calorimeter for showers of 2 GeV. This fixes the energy resolution function over a limited range centered at approximately half of the photon beam energy. With this piece determined, larger opening angles can then be selected, corresponding to asymmetric decays. Choosing the energy cut for shower 1 to be in the range for which the resolution is known and looking at larger opening angles allows knowledge of the single-shower energy resolution function to be extended to low energies. In a similar fashion, the energy resolution function derived for low energy showers can be used to extend the resolution measurement to energies as high as η decays in the 2γ sample allow. The results of this model-independent analysis are shown by the data points in Fig. 4. This model-independent solution was then compared with the standard parametrization [4] of the lead glass energy resolution

$$\frac{\sigma_E}{E} = \frac{B}{\sqrt{E}} + A. \quad (10)$$

The first term on the right in Eq. (10) contains the effects of photoelectron statistics, while the second term wraps up all of the systematic block-to-block differences and calibration errors. A fit of the model-independent resolution data to the form of Eq. (10) in which A and B were allowed to vary freely is shown by the solid curve in Fig. 4.

In order to extend the above analysis to describe the π^0 peak width, it is necessary to introduce a model for the shower spatial resolution. The single-shower spatial resolution function is taken to be proportional to $1/\sqrt{E}$ with a proportionality constant that depends on the geometry of the calorimeter module and must be determined empirically [5]. Eq. (11) is adopted for showers at normal incidence, with the constant C expected to be approximately $7 \text{ mm GeV}^{1/2}$:

$$\sigma_x = \frac{C}{\sqrt{E}}. \quad (11)$$

In the case of showers far from normal incidence, Eq. (11) underestimates shower position measurements because it fails to take into account fluctuations in the centroid caused by shower depth variations. This is taken into

account by projecting one radiation length along the shower axis onto the transverse plane of the calorimeter and adding it in quadrature to the base term in Eq. (11) to obtain the major axis of the error ellipse on the shower centroid. The corrected form of Eq. (11) appears below in Eqs. (15)–(17).

The expression for the variance of m^2 in terms of the variances V_E on the shower energies and V_x, V_y on the shower positions is given by

$$V_{m^2} = \sum_{j=1}^2 \left[\left(\frac{\partial m^2}{\partial E_j} \right)^2 V_{E_j} + \left(\frac{\partial m^2}{\partial x_j} \right)^2 V_{x,j} + \left(\frac{\partial m^2}{\partial y_j} \right)^2 V_{y,j} + 2 \left(\frac{\partial m^2}{\partial x_j} \right) \left(\frac{\partial m^2}{\partial y_j} \right) V_{xy,j} \right] \quad (12)$$

where index j counts photons, and $V_{xy,j}$ is the covariance between the x and y coordinates of the shower centroid for shower j . Eq. (12) can be rewritten in the form

$$\frac{V_{m^2}}{m^4} = \frac{V_E(E_1)}{E_1^2} + \frac{V_E(E_2)}{E_2^2} + \frac{V_s(m^2)}{m^4} \quad (13)$$

where spatial derivatives and variances are grouped into the term $V_s(m^2)$. A lengthy but straight-forward calculation gives V_s in terms of the underlying position uncertainties of the two showers. For example, the contribution from the x coordinate of shower 1 is given by

$$\frac{\partial m^2}{\partial x_1} = -\frac{2p_{z,1}}{z_0 E_1^2} [p_{x,2}(p_{y,1}^2 + p_{z,1}^2) - p_{x,1}(p_{y,1}p_{y,2} + p_{z,1}p_{z,2})] \quad (14)$$

where component $k = 1, 2, 3$ of reconstructed shower $j = 1, 2$ is written $p_{k,j}$. The other spatial derivatives have a similar form and they can be obtained by the proper variable substitution in Eq. (14). The position z_0 of the shower maximum is not directly measured, but from Monte Carlo it is estimated to be about 20 cm into the glass and logarithmically dependent on shower energy. The results of the resolution analysis are not sensitive to changes in z_0 on the order of one radiation length. The fact that departure from normal incidence cannot be ignored requires a treatment of centroid errors that couples the uncertainties in the x and y coordinates. The results are summarized in Eqs. (15)–(17).

$$V_x = \frac{C^2}{E} + (X_0 \sin \theta \cos \phi)^2, \quad (15)$$

$$V_y = \frac{C^2}{E} + (X_0 \sin \theta \sin \phi)^2, \quad (16)$$

$$V_{xy} = X_0^2 \sin^2 \theta \cos \phi \sin \phi. \quad (17)$$

The nominal values of these coefficients are $C = 7.1 \text{ mm GeV}^{1/2}$ and radiation length $X_0 = 31.6 \text{ mm}$ [6], based on the geometry and material properties of the RADPHI calorimeter.

The π^0 sample consisted of 15 M 2γ events selected by limiting the 2γ invariant mass to the range $m < 0.5 \text{ GeV}/c^2$. The corresponding invariant mass distribution is shown on the first panel of Fig. 3. The same distribution is shown in panel 2 of Fig. 3 without the mass cut, but with a shower separation cut of $\gamma > 0.2$ (8 M events) to enhance the η signal. The π^0 and η peaks are fitted with a Gaussian over a polynomial background. Parameters 2 and 3 listed in the figure are the central mass and r.m.s. width of the Gaussian peak returned by the fit. The width of the η peak receives

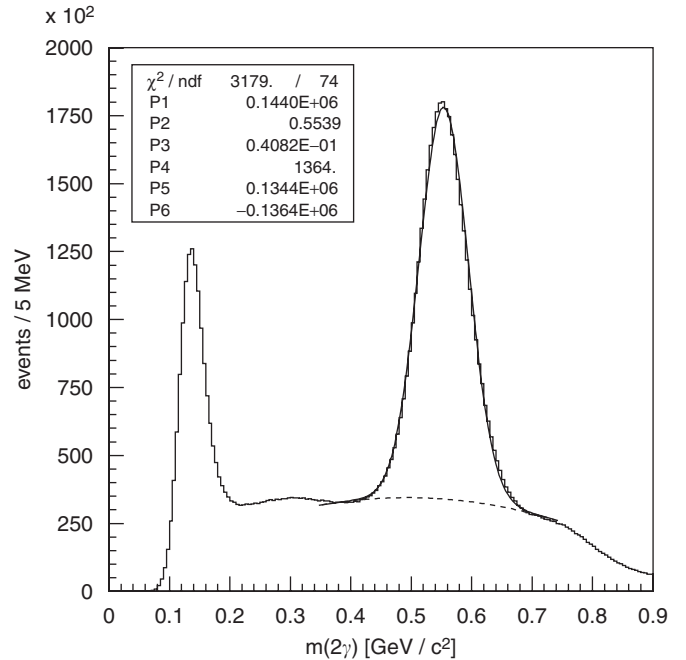
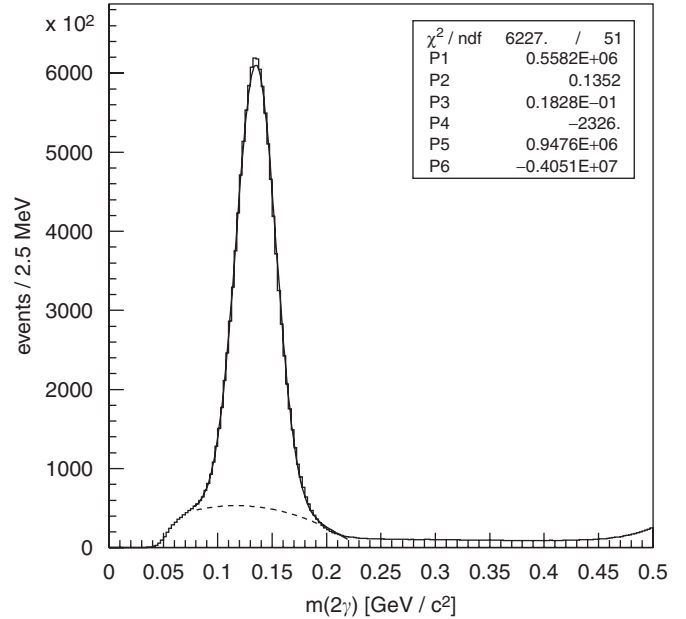


Fig. 3. Invariant mass of reconstructed $\pi^0(2\gamma)$ (first panel) and $\eta(2\gamma)$ (second panel). The parameters shown in the inset boxes are the height (P1), mean (P2) and sigma (P3) of the Gaussian peak fitted to the data over a polynomial background described by parameters P4 + P5 \times m + P6 \times m^2 .

only a few percent contribution from the V_s term in Eq. (13). Neglecting this contribution permitted a model-independent extraction of the energy dependence of the single-shower energy resolution in the calorimeter, as described above, with results shown by the data points in Fig. 4. They are in good agreement with a fit based upon the general form of Eq. (10), indicated by the solid curve in the figure. Extending the fit to include the spatial contribution in Eq. (13) and allowing C to vary as a free parameter leads to the dashed curve in Fig. 4. For most of the energy range the dashed curve lies nearly on top of the solid curve confirming that spatial resolution plays an insignificant role in determining the observed width of the η in this sample.

When the results of the analysis of the η width are applied to the π^0 sample, the predicted widths come out smaller than the measured widths by about 40% when the spatial contribution is neglected. This indicates that the spatial and energy resolution contributions are comparable in the case of the π^0 . A global analysis was applied to both the η and the π^0 samples in which both the energy and spatial contributions to the error were included in a uniform way. A total of 50 measured widths taken from different regions in photon energies and separation angles were used as inputs, and the constants A , B and C from Eq. (10) and Eqs. (15)–(17) were treated as free parameters in the fit. The results of the fit for the energy resolution are shown by the dotted curve in Fig. 4. The

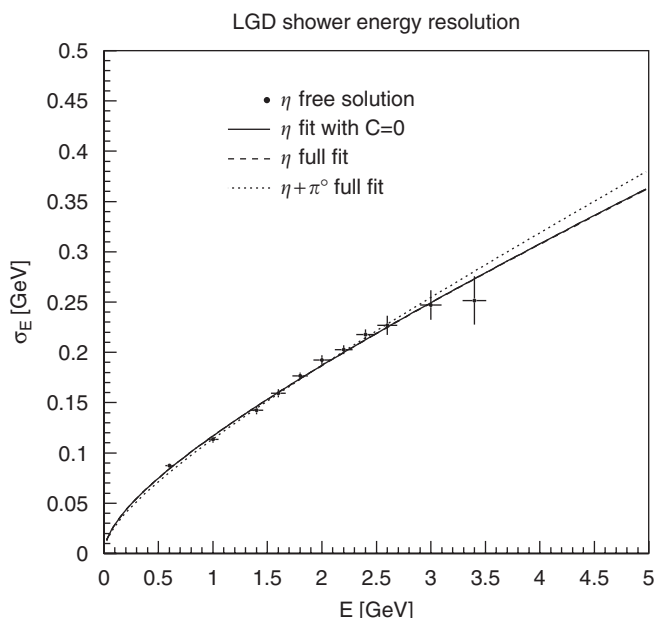


Fig. 4. Energy resolution of showers in the RADPHI LGD obtained from analysis of the 2γ sample. Points represent the free solution to the η squared-mass resolution measurements when the contribution from the spatial resolution has been neglected. The solid line represents the fit to the η data with the standard energy resolution model of Eq. (10). The dashed line represents the fit to these data when the spatial contribution is taken into account according to Eq. (13). The dashed and solid lines are nearly indistinguishable on this scale. The dotted line corresponds to the simultaneous fit to the η and π^0 data with the same resolution function.

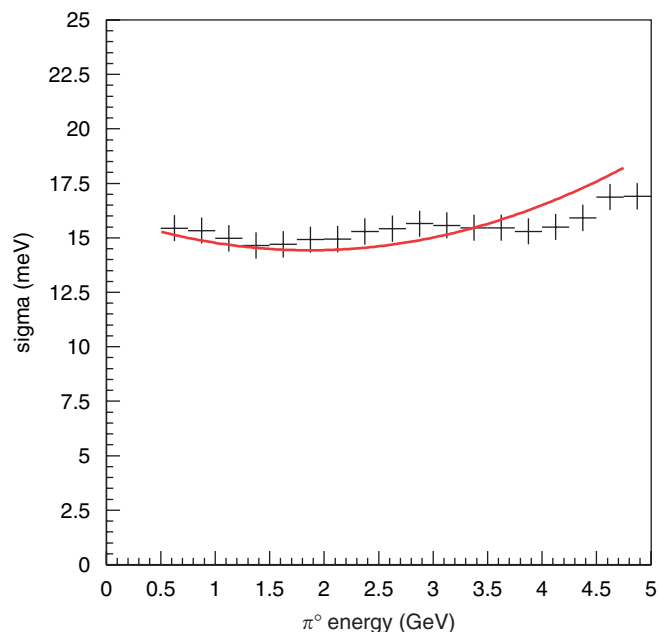


Fig. 5. Standard deviation of the 2γ invariant mass peak for π^0 decays measured with the RADPHI apparatus (data points) as a function of the total lab energy of the decaying particle. The curve indicates the expected width based upon Monte Carlo simulations of this decay.

best-fit values from the fit were $A = 0.035 \pm 0.008$, $B = 0.073 \pm 0.006 \text{ GeV}^{1/2}$ and $C = 6.4 \pm 0.1 \text{ mm GeV}^{1/2}$. The χ^2 returned by the fit is 1.5 per degree of freedom.

The performance of the RADPHI lead-glass calorimeter and this calibration procedure is demonstrated in Fig. 5. The data points are the measured widths of the π^0 peak in the 2γ mass spectrum as a function of the total lab energy of the two-photon system. The curves indicate the expected r.m.s. resolution based upon Monte Carlo simulations. The plot is based upon the sample of all π^0 's from the reaction $\gamma p \rightarrow \omega p$ in the RADPHI data set, reconstructed in the decay mode $\omega \rightarrow \pi^0 \gamma$. It can be seen from this plot that the calibration procedure leads to consistent performance at the expected level across more than a dozen independent calibration periods.

5. Conclusions

We have shown that the reconstruction of electromagnetic showers in a lead-glass calorimeter over a range of incidence angles up to 25° from the normal is possible, provided that corrections to the measured shower energy and position are applied. These corrections are nonlinear functions of both energy and angle and produce significant shifts in reconstructed quantities. We have demonstrated a method for performing a bootstrapped gain calibration of such a lead-glass calorimeter based solely on the analysis of the shape of invariant mass spectra. For the RADPHI experiment, these spectra were derived from the primary data sample and did not require any special calibration runs or triggers. This fact is important because it allows any

changes in the performance of the detector during the experimental run to be taken into account.

In order to evaluate the results of this calibration, the single-shower energy and position resolutions must be measured and compared with established performance benchmarks for lead-glass calorimeters. We have demonstrated a method for measuring the single-shower energy resolution function based only on the shape of invariant mass spectra measured with the calorimeter which allows the resolution to be continuously monitored throughout the duration of a run. The method also provides an independent determination of the shower position resolution under real experimental conditions. The method was applied to the RADPHI data sample, showing a statistical term of $0.073/\sqrt{E}$ in the resolution function that is in agreement with the expectations for lead-glass and a floor term of 0.036. Based on the fact that the floor term contains contributions from other known effects including radiation damage and dead channels that varied across the face of the calorimeter, we estimate the errors on the calibrated gain coefficients to be $\approx 2\%$.

Acknowledgments

This work was supported in part by the U.S. Department of Energy under contract DE-FG02-91ER40661 (Indiana),

the National Science Foundation under grants PHY03-03512, PHY00-72415 (Connecticut), PHY98-03952, PHY00-98674 (Catholic), PHY96-02981, PHY98-04343, PHY00-99557 (William and Mary), PHY99-01133, PHY02-44989, PHY96-03634 (Notre Dame), PHY03-54951 (RPI), PHY99-71970 and PHY01-40230 (Richmond), and the William and Mary Endowment Association. The Southeastern Universities Research Association (SURA) operates the Thomas Jefferson National Accelerator Facility for the United States Department of Energy under contract DE-AC05-84ER40150. We thank S. Denisov for his assistance in obtaining the lead-glass and phototubes used in the initial tests of the calorimeter.

References

- [1] A Measurement of rare radiative decays of the ϕ meson. JLab Experiment E-94-106.
- [2] B.B. Brabson, et al., Nucl. Instr. and Meth. A 332 (1993) 419.
- [3] R. Brun, et al., GEANT User's Guide, Program Library W5013, CERN.
- [4] R. Fruhwirth, et al., Data Analysis Techniques for High-Energy Physics, Cambridge University Press, Cambridge, 2000.
- [5] R. Wigman, International Series of Monographs on Physics, vol. 107, Oxford University Press, Oxford, 2000.
- [6] C.P. Steffen, Ph.D. Thesis, Indiana University, 2001.